Cell Reports, Volume *39*

Supplemental information

The impact of neuron morphology on cortical network architecture

Daniel Udvary, Philipp Harth, Jakob H. Macke, Hans-Christian Hege, Christiaan P.J. de Kock, Bert Sakmann, and Marcel Oberlaender

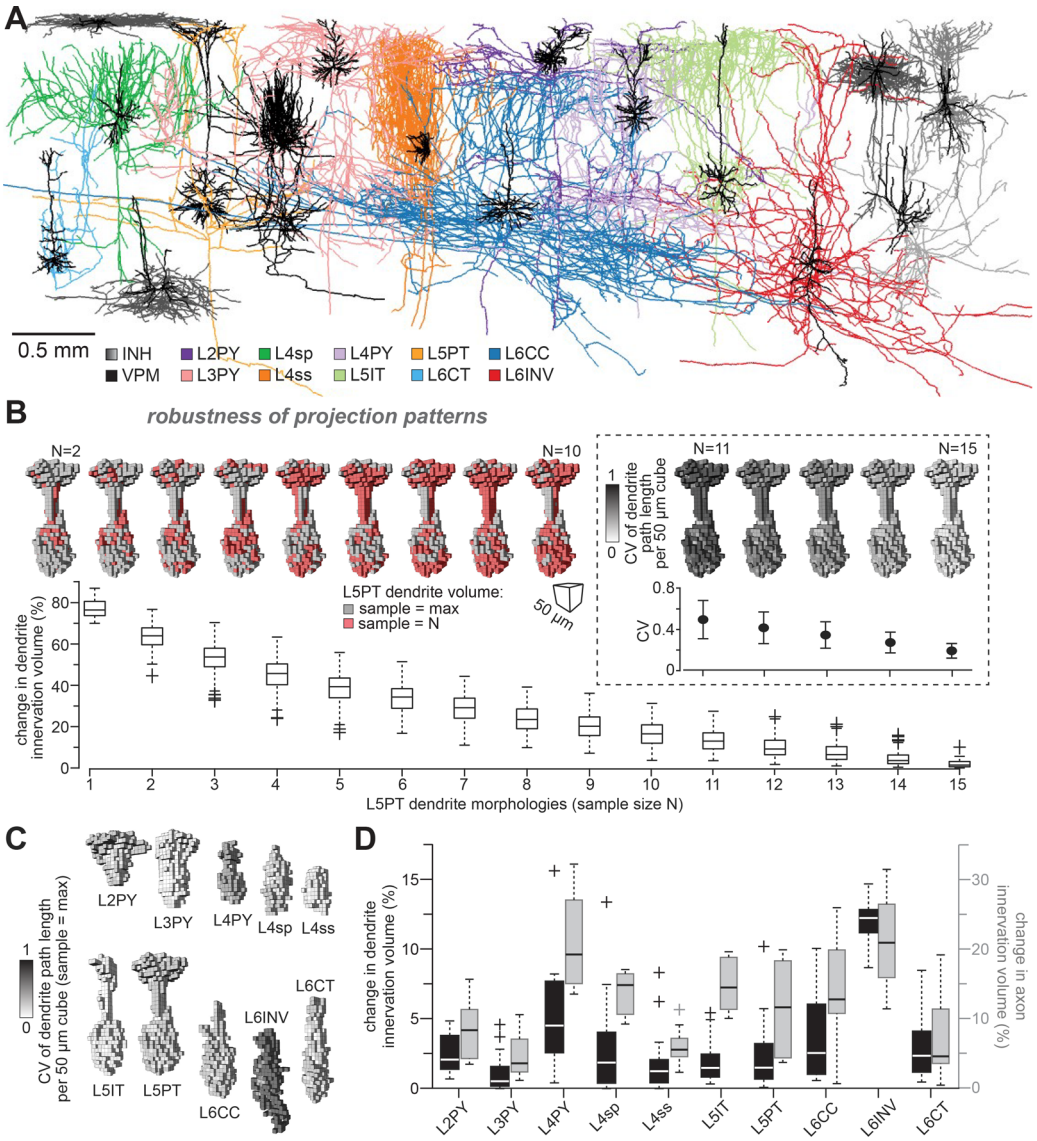

Figure S1 (related to Fig. 1). Robust estimates of dendrite and axon projection patterns. (A) Sample of reconstructed dendrites (black) and axons (modified from (Egger et al., 2020)). Pyramidal neurons in layers 2-4: L2PY (n=16), L3PY (n=30), L4PY (n=7); star pyramids (L4sp, n=15), spiny stellates (L4ss, n=22), slender-tufted intratelencephalic (L5IT, n=18), thick-tufted pyramidal tract (L5PT, n=16), corticocortical (L6CC, n=11) inverted (L6INV, n=5), corticothalamic (L6CT, n=13), and VPM (n=14), and inhibitory neurons (INH) (n=10 *in vivo* (Egger et al., 2015) and 204 *in vitro* (Arzt et al., 2018, Helmstaedter et al., 2009, Koelbl et al., 2015)). **(B)** We investigated how robust the projection patterns of our morphological sample are at a resolution of $(50\ \mu m)^3$. We calculated dendrite and axon innervation volumes for each cell type, while increasing the number of reconstructed morphologies (illustrated here for dendrites of reconstructed L5PTs). The volume innervated by dendrites of L5PTs changes by less than 3% even if additional morphologies were reconstructed. The dendritic path length within each subvolume changes by less than 20%. Insert shows CVs of dendrite densities for each of the subvolumes. **(C)** Innervation volumes and CVs of dendrite densities therein for the maximal sample for each cell type. Similarly low CVs of dendrite densities as for L5PTs. **(D)** Changes of dendrite (black; on average 4%) and axon (grey; on average 12%) innervation volumes for each excitatory cell type at the resolution of 50 µm if additional morphologies per cell type were reconstructed.

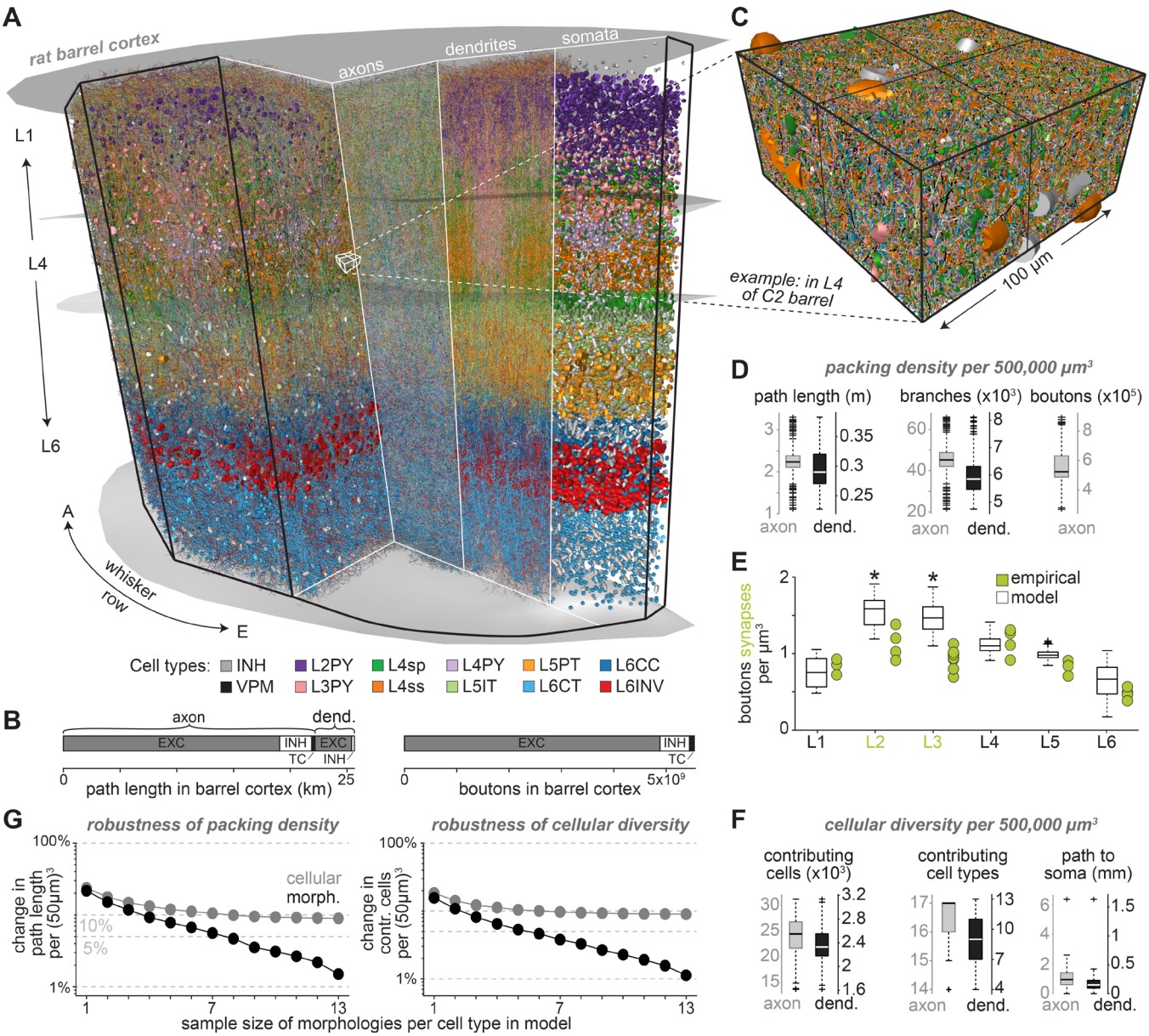

Figure S2 (related to Fig. 2). Validation of the barrel cortex model. (A) Cross-section through the barrel cortex model, illustrating the dense distributions of somata, dendrites and axons (fractions shown), colored by their respective cell types. The model comprises a cortical volume of 6.8 mm^3 (Egger et al., 2012), contains 477,551 excitatory and 69,788 inhibitory neurons, and is innervated by 6,225 neurons from VPM thalamus (Meyer et al., 2013). **(B)** Path lengths of axons and dendrites, and the number of axonal boutons for all excitatory (EXC) and inhibitory (INH) cortical neurons in the model, and thalamocortical (TC) axons from the ventral posterior medial nucleus (VPM). Consistent with early estimates (Braitenberg and Schüz, 1998), the model predicts that 3.3 km of axons and 0.5 km of dendrites are compressed into each cubic millimeter of cortical tissue. **(C)** Zoom-in shows one example subvolume, whose dimensions and location resemble that of the largest densely reconstructed dataset reported so far (Motta et al., 2019). This effort revealed that volumes with such dimensions can comprise more than 45,000 axon and dendrite branches, which represent ~2.7 m of path length and ~400,000 synaptic connections. **(D)** Packing density represented by the path lengths, the corresponding numbers of branches, and the boutons that they represent, for axons

(grey) and dendrites (black) within 500,000 μm^3 large subvolumes (n=128) across the model. The empirical observations by (Motta et al., 2019) fall well within the respective ranges predicted by the model. **(E)** Predicted bouton densities per layer versus synapse density measurements in juvenile rats (Santuy et al., 2018). The differences in layers 2 and 3 between the model and the empirical data (denoted by asterisks) likely reflect age differences (i.e., the data for the model was acquired after postnatal day P28, the empirical data at P14). Synapse densities increase particularly in the upper layers after P14 (Chandrasekaran et al., 2015). **(F)** Cellular diversity here represented by the number of cells that innervate 500,000 μm^3 large subvolumes (n=128) (left), their cell types (center), and location in terms of their path length distance to their somata (right). The 17 cell types reflect VPM, INH (subdivided by layers 1-6) and EXC neurons (subdivided as in panel A). For path to soma only maximum outlier shown. Consistent with the empirical data, the model predicts that >97% of the branches remain unconnected to a soma that lies within the same subvolume. The model thereby provides first insight into the locations and diversity of the neurons from which these unconnected branches originate. **(G)** Quantification of how robustly our reverse engineering approach can predict the packing density and cellular diversity of each subvolume within the barrel cortex model. Left: robustness of the packing density for each subvolume depending on the number of morphologies per cell type that was used to generate the model. Black markers represent the coefficients of variation (CVs) in path length per subvolume across >30,000 models (i.e., median across 125,000 μm^3 large subvolumes), where all models are based on the same average soma distribution (Meyer et al., 2013). Grey markers represent the median CVs for the same subvolumes across models that were based on different empirically measured soma distributions. Right: same robustness analysis for the cellular diversity (i.e., numbers of neurons contributing axonal and/or dendritic branches to each subvolume). The quantification revealed that the packing density in terms of axon and dendrite path length of each subvolume would not change by more than 12% – the cellular diversity by no more than 8% – even if the models were based on a larger sample of reconstructed morphologies. Thus, the model analyzed here provides realistic and robust estimates for the packing density and cellular diversity within any subvolume of the rat barrel cortex.

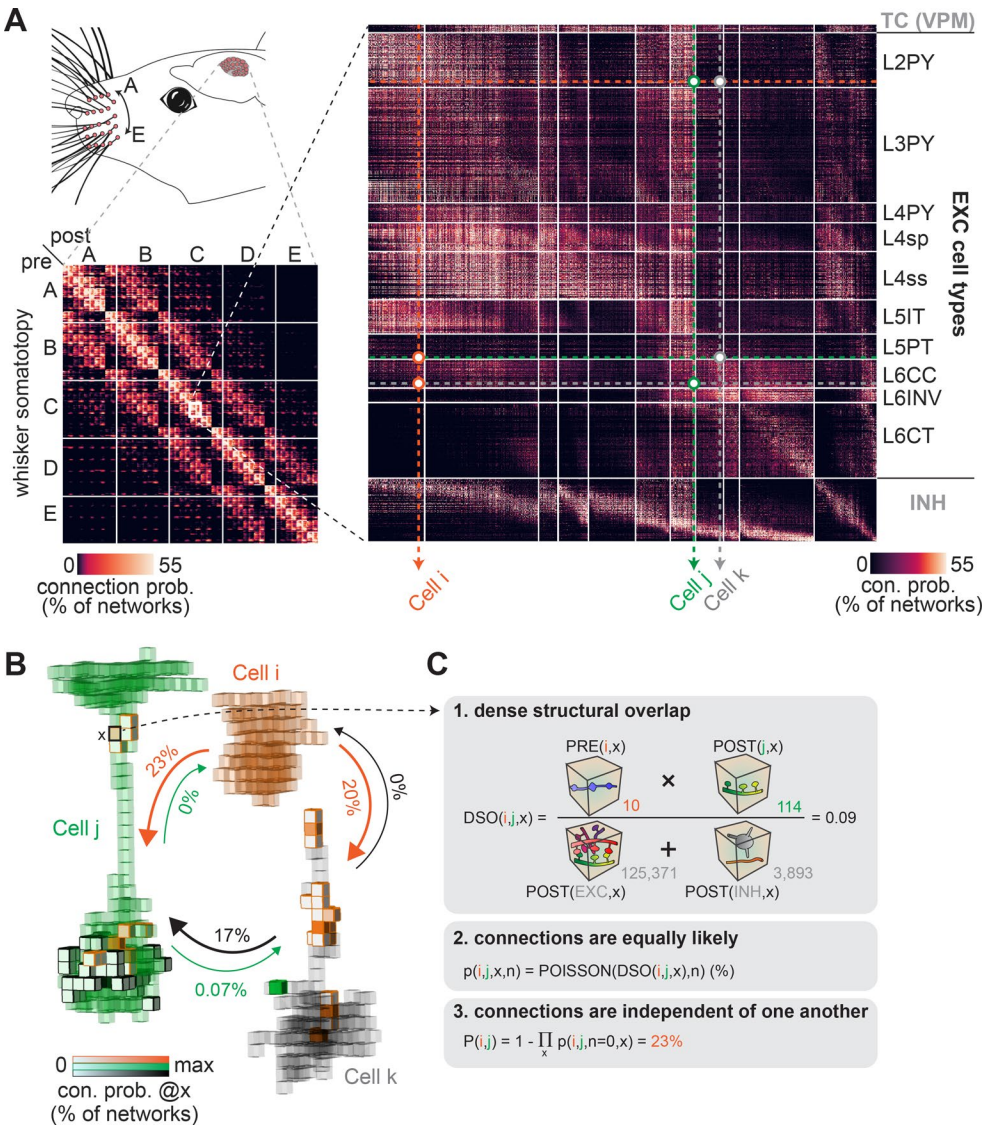

Figure S3 (related to Fig. 2). Ensemble of network configurations for the rat barrel cortex. (A) Matrix representation of the network configurations for the cortical volume that represents the 24 major facial whiskers (i.e., A1-E4, α-δ). Connection probabilities reflect the fraction of networks in which the respective neurons are connected. Right: Zoom-in to the barrel column representing the C2 whisker. The matrix is sorted by soma depth and cell type: VPM (only presynaptic), INH and EXC (subdivided as in **Fig. S2A**). The color map represents 0-95% of the connection probability values (i.e., 0-55%). **(B)** Axo-dendritic overlap between the neurons from panels A and **Fig. 2A** (here at 50 µm resolution). Arrows denote the likelihoods that e.g. the axon of $Cell\ i$ is connected by at least one synapse to the dendrites of $Cell\ j$ within one of their overlap volumes (i.e., in 23% of the networks) when synapse formation mechanisms that introduce wiring specificity are absent (see Equations 2-3 in **STAR Methods**). **(C)** As reported previously (Egger et al., 2014), we parameterize the distributions of pre- and postsynaptic sites by calculating the quantity *dense structural overlap* (DSO) for any subvolume of the barrel cortex model, here illustrated between $Cell\ i$ and $Cell\ j$ in subvolume x at a resolution of 50 µm. This quantity represents the pre- and postsynaptic sites of two neurons in an overlap volume with respect to all postsynaptic sites (see Equation 1 in **STAR Methods**). Excitatory connections are assumed to form between boutons and spines of excitatory neurons, as well as with target sites that

are distributed on the somata and dendrites of inhibitory neurons proportional to their surface areas. For inhibitory connections, target sites on excitatory and inhibitory somata and dendrites proportional to their surface areas are considered, while spines are excluded. Hence, the probability p that two neurons i and j form n synapses in a subvolume x is given by a Poisson distribution with the quantity DSO and n as parameters (see Equation 2 in **STAR Methods**). Thus, $p(i, j, x, n)$ denotes the percentage of networks in which $Cell\ i$ forms n synapses with $Cell\ j$ in subvolume x. Because all connections are assumed to form independently of one another, the probability P that the two neurons are connected in any of the networks by at least one synaptic connection is the product of p across all overlap volumes (see Equation 3 in **STAR Methods**).

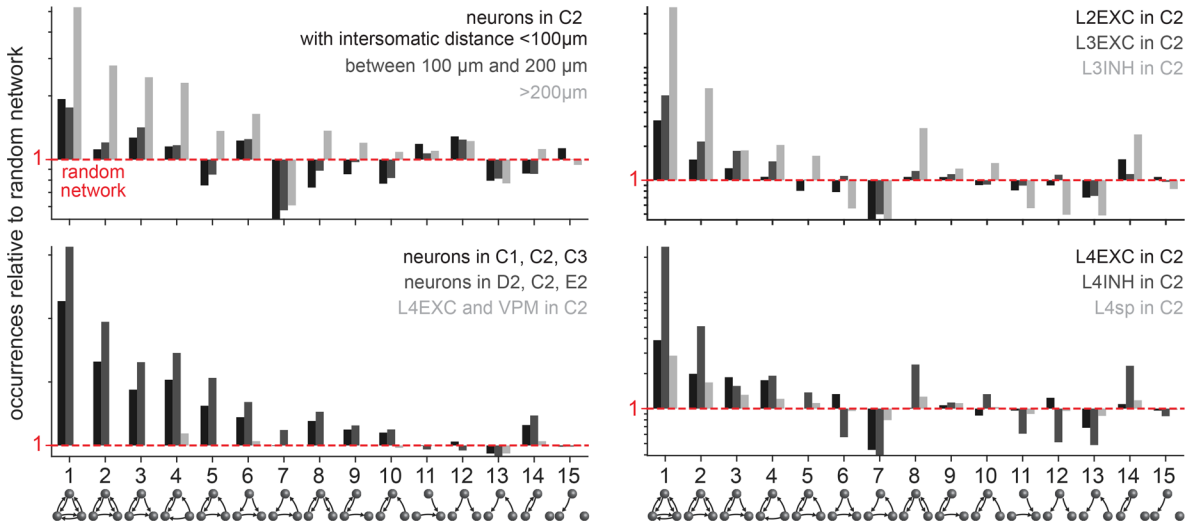

Figure S4 (related to Fig. 3). Occurrences of triplet motifs depend on the grouping of neurons in the barrel cortex model. Ratios between motif occurrences in networks from the barrel cortex model and random networks with the same pairwise statistics for neurons within the C2 barrel column grouped by different inter-somatic distances (top-left), their soma locations in different columns or VPM thalamus (bottom-left), and different neuron populations in layer 2/3 (top-right) and layer 4 (bottom-right). Y-axis in log scale.

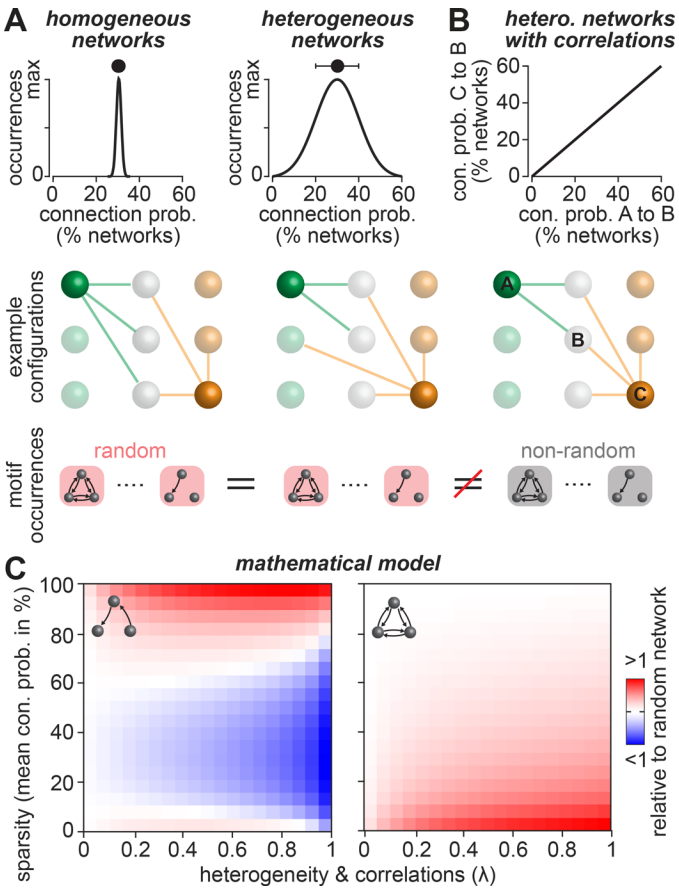

Figure S5 (related to Fig. 4). Mathematical basis for nonrandom motif occurrences. (A) Toy example illustrating Equation 4 in the **STAR Methods**. Left: Homogeneous connectivity (i.e., standard deviation << mean) leads to networks in which all nodes have mostly the same number of edges (here illustrated by two nodes that both have three edges). Right: Heterogeneous connectivity (i.e., standard deviation ≈ mean) leads to networks in which the nodes have on average the same number of edges. Bottom panels: occurrences of triplet motifs will be on average random and identical in all networks that have the same mean connection probability. **(B)** Toy example illustrating Equations 5-6 in the **STAR Methods**. Correlated connectivity (here illustrated by two nodes that both connect to the same nodes) results in networks with motif occurrences that deviate from those of random networks. **(C)** A mathematical model (see **STAR Methods**) that represents networks with correlations reveals how the mean (sparsity) and CV (heterogeneity) of pairwise connectivity impact nonrandom motif occurrences; here illustrated for feedforward chains (left) and recurrent loops (right).

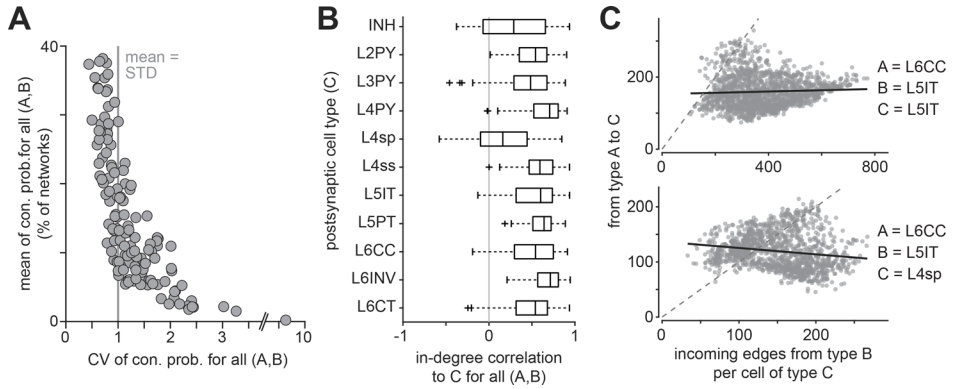

Figure S6 (related to Fig. 4). Pairwise connectivity depends on the grouping of neurons in the barrel cortex model. (A) Means and CVs of connection probability distributions for cell type-specific groupings (10 excitatory cell types, VPM (only presynaptic), and inhibitory neurons; n=132). **(B)** In-degree correlation coefficients for different groupings (n=66 per postsynaptic cell type). All data for neurons closest to the C2 barrel column. **(C)** Correlations between in-degree distributions for three example groupings.

Inter-somatic distance (μm)	Connection probability L5PT to L5PT (%)			
	empirical	predicted		
		median	25th percentile	75th percentile
18	22	23	15	34
53	17	21	13	31
88	15	18	10	28
123	13	15	7	24
158	10	11	4	19
193	10	7	2	14
228	7	4	1	10
263	4	2	0	7
298	7	1	0	6

Table S2 (related to Fig. 6). Predicted versus empirical connectivity data. Inter-somatic distance-dependent connection probabilities between L5PTs. Empirical data from (Perin et al., 2011).

Inter-somatic distance (μm)	Connection probability L2/3EXC to L2/3EXC (%)			
	empirical	predicted		
		median	25th percentile	75th percentile
20	21	30	15	48
60	17	25	11	42
100	13	17	7	32
140	14	11	3	24

Table S3 (related to Fig. 6). Predicted versus empirical connectivity data. Inter-somatic distance-dependent connection probabilities between EXC neurons in layers 2/3. Empirical data from (Avermann et al., 2012).